Improvement of Low Temperature Fracture Toughness of AISI 403 Stainless Steel by Micro Alloying and Heat Treatment

C. Gupta[1], S.L. Wadekar, J.S. Dubey, R.T. Savalia, K.S. Balakrishnan[2], S. Anantharaman[2], Y.V. Kamat[1], and J.K. Chakravartty

Materials Science Division, Bahbha Atomic Research Centre, Mumbai 400 085, India
[1]Department of Production Engineering, Victoria Jubilee Technical Institute, Mumbai 400 019, India
[2]Radiometallurgy Division, Bhabha Atomic Research Centre, Mumbai 400 085, India

ABSTRACT

The effects were studied of a double austenitising and quenching heat treatment and of microalloying with niobium on the low temperature fracture behaviour of AISI 403 stainless steel in the tempered martensitic condition. Instrumented impact tests were carried out on both notched and pre-fatigue cracked Charpy specimens over a range of temperatures. The data obtained were analysed using fracture mechanics principles. The present work indicated that the low temperature fracture process was controlled primarily by the martensitic packet size which influenced micro-cleavage fracture stress significantly. Both heat treatment and microalloying refined the martensitic structure which resulted in the improvement of dynamic fracture toughness in the lower shelf regime and in lowering of the ductile to brittle transition temperature.

INTRODUCTION

AISI 403 stainless steel in tempered martensitic condition has been chosen as endfitting material for Pressurized Heavy Water Reactors (PHWR) due to its excellent high temperature corrosion resistance, good elevated temperature mechanical properties and moderate irradiation resistance /1,2/. In addition to these attributes, this variety of stainless steel possesses coefficient of thermal expansion values which match that of zirconium alloy pressure tube materials to give a leak tight joint established by mechanical rolled joining technique. This latter attribute makes these steels almost indispensable as end fitting materials /2/. However, major disadvantages with these steels are their low ambient temperature toughness and relatively high ductile to brittle transition temperature (DBTT) which is near ambient /1,2/. When end fittings are exposed to high neutron flux during their service, the fracture toughness is lowered and the DBTT is increased with increasing fluence /3/. As a result of these factors, their susceptibility to brittle cleavage fracture is enhanced. From an engineering point of view, it is therefore preferable to use a material with high initial toughness and a lower DBTT in order to reduce the susceptibility to brittle catastrophic failure.

In a previous study, the effect of microstructure on room temperature and fracture behaviour of this steel was investigated /4/. It was found that both grain size and carbide shape, size and distribution influence fracture toughness significantly. In this respect, a double quenching and tempering treatment which refined the grain structure and produced a preferred carbide morphology was found suitable to improve toughness compared to conventional tempered martensite microstructure of the same base steel. Similar efforts have also been made earlier by other researchers to characterize the room temperature fracture behaviour of this material. However, virtually no attempt has been made to characterize the fracture behaviour at low temperatures where this material fails

essentially in a brittle manner. This is important, as a knowledge of the resistance to brittle fracture is essential in the design of structural materials for nuclear reactors. Further, investigation on the effects of microstructure on the low temperature fracture behaviour is quite limited for this variety of steels. From a material science point of view, in order to improve low temperature toughness, it is essential to understand the effect of various microstructural features on the low temperature fracture behaviour.

The objective of the current investigation is further to improve the low temperature fracture toughness of the base AISI 403 steel through microstructural control via modifications by microalloying and heat treatments. In addition, an attempt will also be made to identify the microstructural parameter that controls low temperature fracture behaviour on a microscopic scale. For the purpose of characterising low temperature fracture behaviour, fracture mechanics principles have been employed and instrumented impact testing has been carried out on both notched and fatigue precracked Charpy specimens over a range of temperature. Two different methods, namely a special heat treatment /4/ and microalloying by niobium, have been employed for improvement of toughness. Both these methods are expected to refine the microstructure of AISI 403 steel. The basic microstructure will be tempered martensitic in all the cases to be studied; however, there will be variations in terms of carbide morphology and grain size of the ferritic units. Finally, the results obtained in this investigation are discussed on the basis of the existing models of brittle (cleavage) fracture.

EXPERIMENTAL

Two different variants of AISI 403, namely the conventional and the niobium modified varieties, were studied in this work. Compositional details of these materials are given in Table 1. The conventional AISE 403 material was received in the form of forged blocks which were oil quenched from 910°C (±10°C) and subsequently tempered at 610°C (±10°C) for 4 hrs (designated as QT). The niobium modified variety was in forged condition without any heat treatment. A part of the QT material was subjected to special heat treatment which consisted of the following steps: i) oil quenching from 1040°C after soaking for 30 minutes, ii) second oil quenching from 850°C after 30 minutes holding on rapid heating to soaking temperature, and finally iii) tempering at 610°C for 4 hrs followed by water quenching. The double quenched material will be designated as DQT. The niobium containing material was given conventional hardening (950°C, 45 minutes soaking following by an oil quench) and tempering (670°C, 4 hrs) to generate tempered martensitic structure (designated as NQT). The hardness of QT and DQT material was in the range of 260 to 275 VPN. The tempering temperature of NQT material was chosen to obtain an upper shelf energy comparable to QT and DQT materials /4,5/. Upon completion of the heat treatment, mechanical test specimens were finished machined from each of the three heat treated materials.

The microstructures of all the heat-treated conditions were examined using optical microscopy (OM), scanning electron microscopy (SEM) and transmission electron microscopy (TEM). OM was used primarily to determine grain size (both prior austenite

Table 1
Chemical composition of materials under study (wt%)

Element	AISI 403 (conventional)	AISI 403 (Nb modified)
C	0.1-0.12	0.1-0.11
Cr	11.5 - 12.5	11.5 - 12.5
Mn	0.25	0.2
Si	0.16	0.18
S and P	< 0.02	< 0.02
Nb		0.1 - 0.2

grain size and martensitic packet size). The SEM was employed to reveal carbide distribution and morphologies on etched metallographic sections. TEM investigations furnished morphological details of the tempered martensitic microstructures that had been produced, as well as sizes and distribution of carbide particles.

Both transversely oriented cylindrical tensile samples (with gauge length of 25 mm and diameter of 6 mm) and ASTM Standard Charpy impact test specimens (10 x 10 x 55 mm) were machined from the heat-treated blocks. Tensile tests were carried out in a screw driven machine using a strain rate of $10^{-4}s^{-1}$. All impact tests were carried out on Charpy specimens using a 360 Joule Capacity Tinius Olsen instrumented impact testing machine in accordance with ASTM E 23-86 standard test procedure. Both notched and prefatigue cracked specimens were used. Fatigue precracking of Charpy specimens were done as per the recommendations of ASTM test standard for J_{IC} testing E 813-89) and precracking was continued till a ratio of crack length to width, a/w of 0.5 to 0.6, was obtained. Impact tests on notched specimens were carried out over a temperature range of –196°C to 250°C while prefatigue cracked samples were tested in the temperature range –100°C to 250°C. Dynamic load-time and energy-time records which were obtained at various temperatures were used for estimating the ductile to brittle transition temperature, fracture (or maximum) load, general yield load and the energies corresponding to the various stages of fracture process. The details of the methodology for evaluation of these parameters are given elsewhere /6,7/.

The fracture surface morphology of impact tested samples was examined using standard techniques of fractographic analysis using scanning electron microscopy.

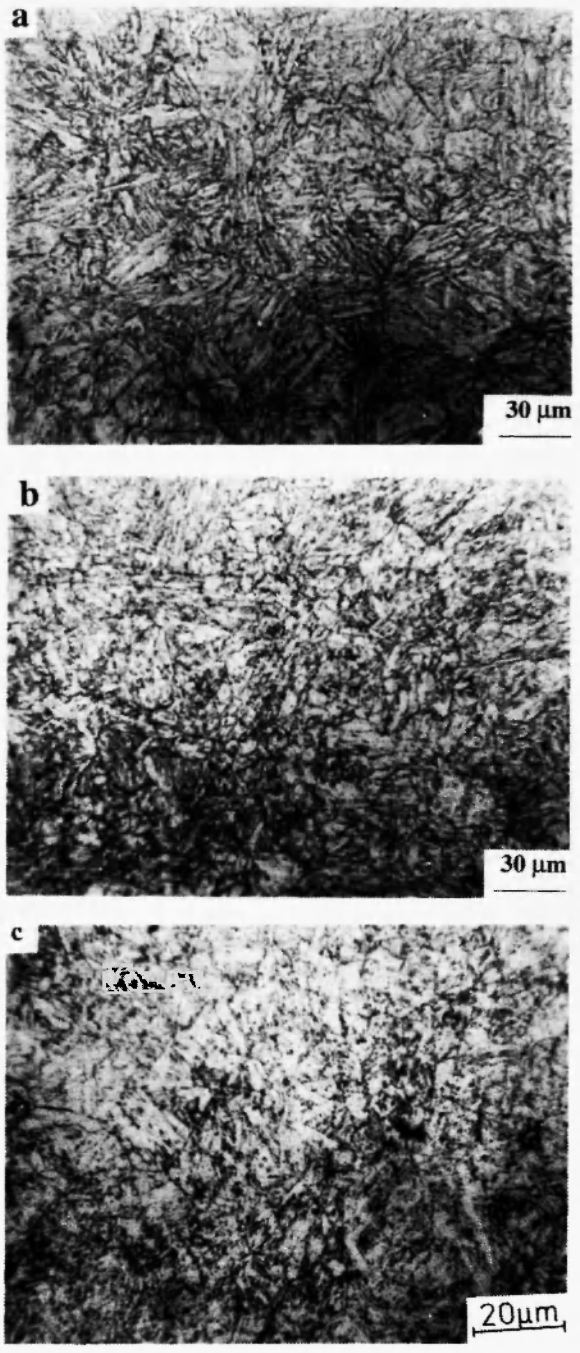

Fig. 1: Microstructure produced by different heat treatments of AISI 403 stainless steel etched in 2% picral: a) As received materials (QT); b) Double quenched material (DQT) and c) Niobium modified material (NQT). Optical micrographs (a-c) show tempered martensitic structures with different prior austenite grain sizes.

RESULTS AND DISCUSSION

Light micrographs (Fig. 1) show the microstructures produced in different heat treatments QT, DQT and NQT. They all exhibit tempered martensitic microstructure. It is seen that DQT treatment and microalloying have refined the grain structure compared to that in the QT material. The difficulty in

distinguishing the packet boundaries from prior austenite grain boundaries resulted in considerable scatter in the measured values of the grain sizes produced by these heat treatments (Table 2). However, it is clear that DQT treatment has produced the finest microstructure, followed by NQT. Full morphological details of the microstructure produced have been studied by TEM and are given elsewhere /4,5/. Some observations of importance with respect to the present work are summarized below: The martensites produced by these heat treatments are of lath type and contain a high density of dislocations within them. The individual laths have widths in the range of 0.4 to 0.6 μm, tempering subsequent to quenching resulted in annihilation of dislocations by recovery and formation of different types of carbide morphology and distribution. In QT material, the carbides are primarily of lenticular shape and are located primarily at the prior austenite grain boundaries, at the packet boundaries and also at the lath boundaries. In DQT and NQT materials, on the other hand, the carbides appear to be of lower aspect ratios than QT material and are more homogeneously distributed. Selected area diffraction analysis revealed that carbides were predominantly $Cr_{23}C_6$ type.

The results of the room temperature tensile tests on these materials are given in Table 2. It is seen that the DQT treatment has not altered the strength significantly but has improved the ductility considerably and also the value of work hardening exponent compared to that of the QT structure. Microalloying by niobium has brought a significant improvement in strength with marginal loss of ductility compared to the QT structure. Table 2 also compares the DBTT (temperature corresponding to 41 J) of these materials. A dramatic improvement in toughness, as indicated by the lowering of DBTT, results from DQT treatment while only a moderate improvement results from NQT treatment. The details of this improvement in room temperature mechanical properties have been reported and rationalized on the basis of the observed microstructural features, namely grain size and carbide morphology, elsewhere /4,5/. In the following sections, we shall deal with the low temperature fracture behaviour.

In this investigation the concepts of stress intensity factor (K) and J-integral of Rice /8,9/ are applied to characterize the low temperature fracture behaviour. The dynamic initiation toughness, K_{Id}, for all the three materials was determined using the following expression /10?:

$$K_{Id} = [6M/(BW^2)]\, a_o^{1/2}\, f(a_o/W) \qquad (1)$$

where K_{Id} is in MPa$\sqrt{m}$, P is the peak load in kN, a_0, W, B are the initial crack length, width and thickness of the impact samples (in cm) respectively. M is the bending moment given as PL/4; where L = 4W and $f(a_0/W) = 1.93 - 3.07\,(a_0/W) + 14.53\,(a_0/W)^2 - 25.11\,(a_0/W)^3 + 25.8\,(a_0/W)^4$.

J-integral values were computed using Rice's estimation formula corresponding to the maximum load supported by a deeply precracked specimen. The original expression for J integral given by Rice can be reduced to the following working relationship to estimate

Table 2
Room temperature mechanical properties of the materials used

Material	DBTT* (°C)	Yield strength (MPa)	Ultimate tensile strength (MPa)	Total elongation (%)	Work hardening exponent	Grain size** (μm)
QT	50	580 - 640	690 - 710	17 - 20	0.08	48 ± 8
DQT	- 20	600 - 630	700 - 730	24 - 28	0.12	17 ± 5
NQT	10	695 - 720	780 - 810	13 - 16	0.08	32 + 5

* Ductile to brittle transition temperature at 41 J.

** Prior austenite grain size as measured by linear intercept method from optical metallographs and scanning electron micrographs.

the dynamic fracture toughness at peak load /8/,

$$J_{pd} = 2E_p / [\, B\,(W-a_o)] \qquad (2)$$

where E_p is absorbed energy up to the peak load. The critical stress intensity factor was also evaluated from the critical value of the J integral (J_{pd}),

$$K_{pd} = (J_{pd}\, E\,)^{1/2} \qquad (3)$$

where E is the Young's modulus.

The variation of K_{ID} with temperature for all the three materials is shown in Fig. 2. The toughness values increase with increasing temperature and each of the plots shows three distinct regions similar to the impact energy vs. temperature plot showing typically an upper shelf, a transition region and a lower shelf regime. A K_{Id} value below 50 MPa$\sqrt{m}$ satisfies the validity criteria of ASTM E-399, for the specimen size used in this investigation. The temperature corresponding to this toughness level may be considered as the temperature of transition from brittle to ductile behaviour. The respective transition temperatures (T_k) for the three materials are shown in Table 3. The trend in the variation of this transition temperatures as a function of microstructure is similar to that obtained by impact testing of notched samples (Table 2). Similar variation of toughness with temperature is also seen in the plots of J_{pd} vs. temperature for these materials in Fig. 3, which also depicts a clear three stage behaviour.

Also included in the same plots are values of K_{pd} obtained by using equation (3). It may be noted that K_{pd} values corresponding to lower shelf level are much higher than the corresponding K_{Id} obtained from equation (1). This difference stems from the fact that the energy level corresponding to maximum load represents energy actually involved for finite crack extension rather than at zero crack extension /11,12/. Furthermore, for computing J_{pd} values corrections due to

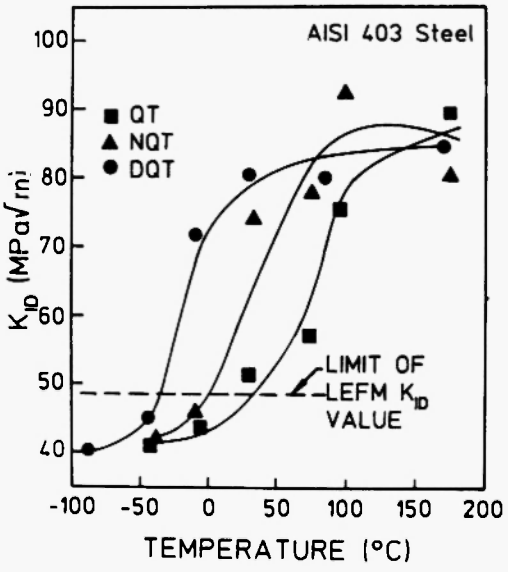

Fig. 2: Variations in dynamic fracture toughness (K_{Id}) values of the three materials with temperature.

Table 3
Cleavage fracture related parameters of the materials studied

Material	T_k* (°C)	Facet size (μm)	Cleavage Fracture stress (MPa)	Characteristic distance (l*) (μm)	σ_f^* (Griffith) (MPa)
QT	35	9 -12	≈ 1750+	52	1880
DQT	0	4 -6	2550	20	2650
NQT	-35	7 - 10	2220	34	2100

* T_k is the transition temperature at K_{Id} = 50 MPa$\sqrt{m}$

+ taken from an unpublished work/28/

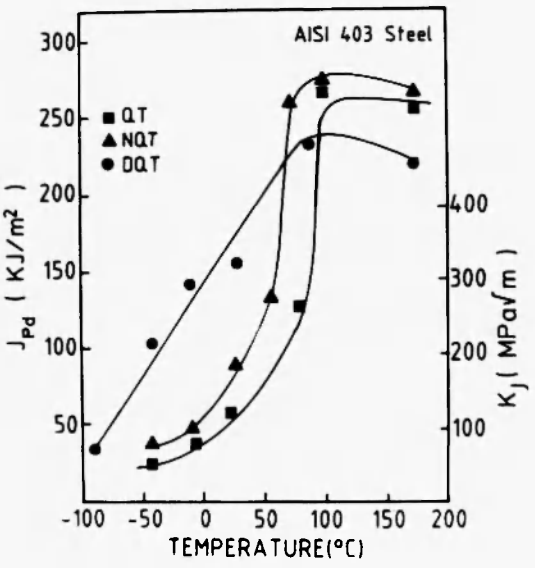

Fig. 3: Variation in dynamic fracture toughness measured in J-integral format (J_{pd}) of the three materials with temperature.

specimen deflection were not taken into consideration in this investigation /13/. Irrespective of the correctness of the values of toughness measured as J_{pd}, it is clear that both the measures of fracture toughness (J_{pd} and K_{Id}) have ranked the microstructures in terms of their resistance to brittle fracture in the following sequence of decreasing fracture toughness: DQT > NQT > QT. The mode of brittle fracture for all the materials used for this investigation in the region below the valid K_{Id} level is transgranular quasi-cleavage (Fig. 4) where the fracture surface is found to consist of distinctive cleavage facets, dimples as well as tear ridges, and further the dimpled areas join the cleavage facets to each other. The extent of these ductile ridges has been found to increase with temperature in the lower shelf region. Similar observations have also been made earlier in the case of brittle cleavage failure of many quenched and tempered steels /14-16/. Cleavage fracture in lath martensitic as well as bainitic structure is

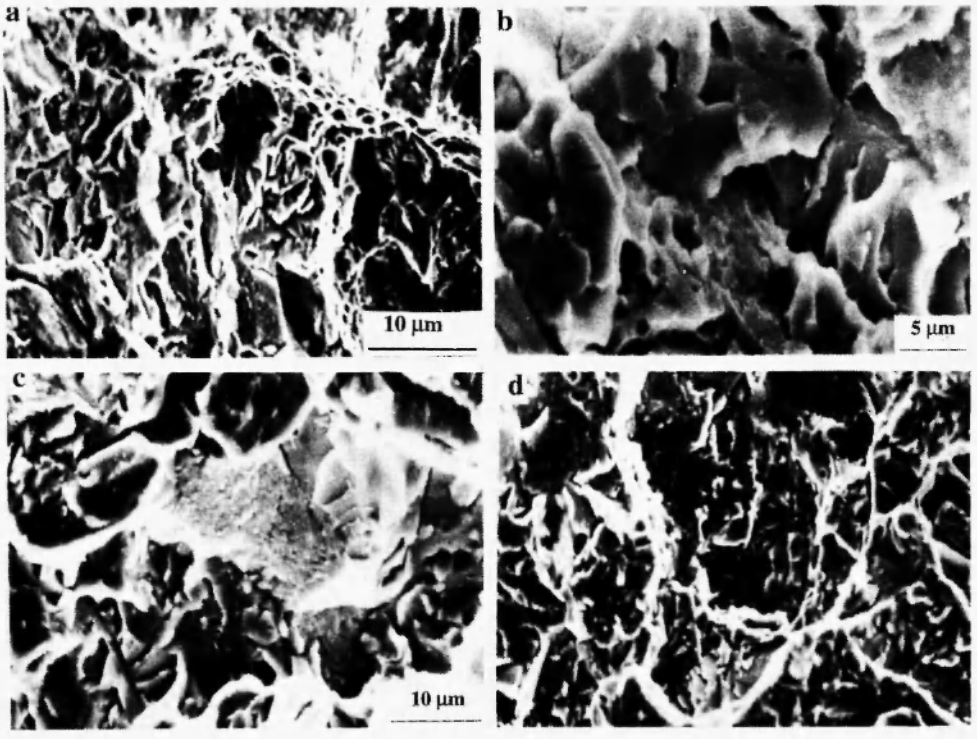

Fig. 4: Fracture surface morphologies of the three materials tested at temperatures corresponding to their lower self regime: a) DQT material tested at –50°C, showing cleavage facets, dimpled areas and tear ridges; b) DQT material tested at –90°C, showing cleavage facets; c) NQT material tested at –40°C, showing cleavage facets and tear ridges joining adjacent facets and d) QT material tested at –40°C, showing large cleavage facets.

believed to occur by the formation of microcracks which tend to be arrested at packet boundaries and also by the propagation of packet sized microcracks /17,18/. The cleavage facets observed in Fig. 4 should then roughly correspond to packet morphology. Facet sizes have been measured from fractographs such as those in Fig. 4 and are given in Table 3. It is seen that the smallest facet size is associated with DQT structure which showed lowest DBTT and also highest K_{Id} value at any given temperature. These observations support the general trend that fine grained materials possess superior toughness in tempered martensitic conditions /17,19/. It is pertinent to mention here that neither carbides nor any inclusions were involved in the fracture process, as established by detailed fractographic analysis.

It is now necessary to identify the principal microstructural features that control the resistance to cleavage fracture of the three microstructures on a microscopic scale. Cleavage fracture is commonly accepted to be stress controlled and occurs when the macroscopic applied tensile stress (σ_n) exceeds a critical microcleavage stress (σ_f^*) over a critical distance /20/. Using this mechanistic model of cleavage failure Ritchie, Knott and Rice (RKR) /20/ were able to relate lower shelf toughness values to the fracture stress (σ_f^*), the yield stress (σ_o) and the characteristic microstructural parameter (l*). In this work σ_f^* has been estimated from general yield load (P_{gy}) and maximum load (P_m) data obtained from notched impact tests over a range of temperatures. Noting the value of P_{gy} at $P_{gy} / P_m = 0.8$, σ_f^* was obtained by using a relationship given by Wullaert /21/,

$$\sigma_f^* = 112.5\ P_{gy} \qquad (4)$$

where σ_f^* is in MPa and P_{gy} in kN. A typical plot of P_{gy} and P_m (or P_f) as a function of temperature is shown in Fig. 5 for DQT structure. The value of σ_f^* determined from data in this way for the three materials is given in Table 3. Here again we note that the higher value of σ_f^* is associated with a finer microstructure. These σ_f^* values can now be used to compute characteristic microstructural distances, l*, from the K_{Id} values obtained earlier (Fig. 2), using an approach suggested by Odette *et al.* /22,23/. Odette and coworkers have shown that stress field ahead of a crack tip can reasonably be represented by spline fits of the form $\sigma_n / \sigma_o = A - B * (K/\sigma_o)^2$. Using the RKR model /20/ and noting that the critical point $\sigma_n = \sigma_f^*$ and $K = K_{IC}$ (or K_{ID}), an expression for toughness can be obtained as

$$K_{Id} = [\, B\sigma_0^2 l^* / (\, A - \sigma_f^* / \sigma_o\,)\,]^{1/2} \qquad (5)$$

where A and B are stress field parameters and depend on the values of work hardening exponent (n), yield strength (σ_o) and Young's modulus (E). Appropriate stress field parameters for this steel ($n \doteq 0.1$ and $\sigma_o/E < 0.01$ (will be A = 4 and B = 100 /22/. In computing l* for the three materials the following data were used: for DQT, K_{Id} = 40 MPa$\sqrt{m}$ at –90°C, for NQT, K_{Id} = 42 MPa$\sqrt{m}$ at –40°C, and for QT, K_{Id} = 43 MPa$\sqrt{m}$ at –10°C.

σ_O values were taken as dynamic yield strength (σat the appropriate temperatures and were obtained from P_{gy} values using the relation $\sigma_{yd} = 51.6\ P_{gy}$ where σ_{yd} is in MPa and P_{gy} in kN /24/. The computed l* values are shown in Table 3. The values of l* so obtained approximately match the size of prior austenite grains of the three materials. The value of σ_f^* and l* obtained in this work are consistent with the available data on quenched and tempered low alloy steels having similar subgrain structures. These results are also in agreement with an earlier work on 12% Cr martensitic steel (HT-9) where l* was found to be approximately equal to the

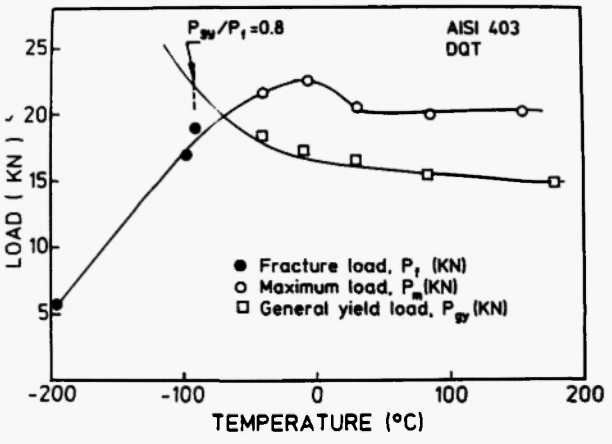

Fig. 5: Plots of general yield load (P_{gy}), fracture load (P_f) and maximum load (P_m) as a function of temperature for DQT material.

prior austenite grain size and is independent of temperature /22,23/. In this work no attempt was made to establish the strain rate and temperature independence of l^* and σ_f^* since there is a large volume of work on different types of steels to support this observation /16,22,25,26/. The observation that the computed values of l^* are nearly equal to prior austenite grain sizes of the respective microstructures is suggestive of the fact that these boundaries are possible sites for crack initiations. Cleavage fracture, in bainitic and martensitic steels where carbides have usually been observed not to control the fracture process, would seem to be controlled primarily by the martensite/ bainite packet size /17,18/. It is thus expected that the size of the cleavage facets will be determined by the packet size and the possible critical stage in the fracture process may involve propagation of a 'packet-size' micro-crack. The micro-cleavage fracture stress σ_f^* can be related to controlling microstructural features through a modified Griffith's equation of the form,

$$\sigma_f^* = [(4E \gamma_p) / (\pi (1- \nu^2) x)]^{1/2} \quad (6)$$

and using E = 210 GPa, effective surface energy (γ_p) = 120 J/m^2 for bainitic and martensitic steels /17/, ν = 0.3 and x = packet diameter. The predicted σ_f^* values agree well with experimentally determined cleavage fracture stress values (Table 3) and are related to packet size (d_p) by $\sigma_f^* \approx C (d_p)^{-1/2}$, where C is a constant. The present results are consistent with earlier work reported by Odette and co-workers on tempered martensitic stainless steels /22,23/ and lend support to a semi-quantitative model proposed by Knott /27/ suggesting that the microcleavage fracture stress is controlled by propagation of a packet size crack through adjoining martensite laths which fail by ductile internal necking process.

CONCLUSION

The present work shows that the resistance to cleavage fracture is controlled by the packet size of the tempered martensitic structure in AISI 403 steel. Refining the packet size improves low temperature fracture toughness by enhancing the microcleavage fracture stress. Both double quenching and micro-alloying with niobium have been found suitable for improving low temperature fracture toughness.

ACKNOWLEDGMENT

This investigations forms a part of a general research programme on the mechanical properties of nuclear structural steels. We are grateful to Dr. S. Banerjee for his keen interest in this work and for his valuable comments during the preparation of the manuscript. The authors would also like to tender their sincere thanks to Mr. S. Chaterjee for valuable discussion and for providing some unpublished data.

REFERENCES

1. R.R. Hobsons and J.K. Macpherson, in: *Materials in Nuclear Energy*. [[_____]]], Ohio, 1982; p. 37.
2. R.R. Hobsons, A.J. Percy and B.I. Wotton, *Properties of Reactor Structural Alloys After Neutron or Particle*, ASTM STP 570, American Society for Testing and Materials, Philadelphia, 1975; p. 103.
3. D.C. Douglass, "The metallurgy of zirconium", *Atomic Energy Review*, 1971.
4. C. Gupta, J.S. Dubey, S. Ganguly, A.R. Biswas, Y.V. Kamat and J.K. Chakravartty. Accepted for publication in *High Temperature Materials and Processes*, 1996.
5. C. Gupta, M.Tech. thesis "Improvement of toughness of end fitting material in pressurized heavy water reactor", Victoria Jubilee Technical Institute, Mumbai, October, 1996.
6. S. Chatterjee, S. Anantharaman, U.K. Viswanathan and K.S. Sivaramakrishnan, *ASTM STP*, **536**, 231 (1973).
7. S. Chaterjee, H.K. Sriharsha and U.K. Viswanathan, *ASTM STP*, **1175**, 211 (1993).
8. J.R. Rice, P.C. Paris and J.G. Merkle, *ASTM STP*, **536**, 231 (1973).
9. W.L. Server, *J. Testing and Evaluation*, **6**, 29 (1978).

10. T.J. Koppennal, *ASTM STP*, **563**, 92 (1974).
11. T. Kobayashi, *Engg. Fract. Mech.*, 19(1), 49 (1984).
12. H. Takahashi, M.A. Khan and [[_____]] Suzuki, *J. Testing and Evaluation*, 8, 63 (1980).
13. R.J. Buzzard and D.M. Fisher, *J. Testing and Evaluation*, 6, 35 (1978).
14. J.F. Knott, *Trans. ISIJ*, **21**, 305 (1981).
15. M.K. Veistinen, T.K. Salmi and V.K. Lindroos, *Scand. J. Metallurgy*, **13**, 259 (1984).
16. P. Bowen and J.F. Knott, *Metal Sci.*, **18**, 225 (1984).
17. P. Brozzo, G. Buzzichelli, A. Mascanzoni and M. Mirabile, *Met. Sci.*, **11**, 123 (1977).
18. G.G. Chell and D.A. Curry, "Mechanics and mechanisms of cleavage fracture", in: *Developments in Fracture Mechanics*, Volume 2, G.G. Chell (ed.), Applied Science Publishers, 1991; p. 101.
19. J.P. Naylor and R. Blondeau, *Metall. Trans.*, 7A, 891 (1976).
20. R.O. Ritchie, J.F. Knott and J.R. Rice, *J. Mech. Phys. Solids*, **21**, 395 (1973).
21. R.A. Wullaert, *ASTM STP*, 466, 148 (1970).
22. G.R. Odette and G.E. Lucas, *J. Nucl. Materials*, **117**, 264 (1983).
23. G.R. Odette, G.E. Lucas, R. Maiti and J.W. Shackherd, *J. Nucl. Materials*, **122/123**, 442 (1984).
24. A.P. Green and B.B. Hundy, *J. Mech. Phys. Solids*, 4, 128 (1965).
25. R.O. Ritchie, W.L. Server and R.A. Wullaert, *Metall. Trans.*, **10A**, 1557 (1979).
26. R.A. Fernandes, F.A. Darwish and J.C.G. Teixeria, in: *Fracture Prevention in Energy and Transport Systems*, Vol. II. Lain Le May and S.N. Monterio (eds.). EMAS, Engg. Mats. Advisory Services Ltd., Warley, U.K., 1983; pp. 583-591.
27. J.F. Knott, in: *Conference on Fracture Mechanics in Design and Services – Living with Defects*, Royal Society, London, 1979.
28. U.K. Viswanathan, S. Anantharaman and s. Chatterjee, Internal Report "Charpy impact test on nuclear structural materials from Nuclear Power Board", Bhabha Atomic Research Centre, India, 1987.